International Journal of Applied Mechanics
Vol. 15, No. 2 (2023) 2350009 (20 pages)

DOI: 10.1142/S1758825123500096

The Optimum Inertial Amplifier Tuned Mass Dampers for Nonlinear Dynamic Systems

Sudip Chowdhury* and Arnab Banerjee†

Civil Engineering Department
Indian Institute of Technology, Delhi, India
**sudip.chowdhury@civil.iitd.ac.in*
†abanerjee@iitd.ac.in

Sondipon Adhikari

James Watt School of Engineering
The University of Glasgow, Glasgow, UK
Sondipon.Adhikari@glasgow.ac.uk

Received 19 September 2022
Accepted 15 November 2022
Published 19 January 2023

The optimum inertial amplifier tuned mass dampers (IATMD) for vibration reduction of linear and nonlinear dynamic systems are introduced in this paper. H_2 and H_∞ optimization methods are applied to derive the exact closed-form expressions for optimal design parameters such as frequency and viscous damping ratios in simplified form mathematically for IATMD. From the parametric study, using these optimal closed-form solutions, a higher damper mass ratio, a higher amplifier mass ratio, and a lower inertial angle are recommended to design optimum IATMD to achieve robust dynamic response reduction capacity having moderate viscous damping and lower frequency ratios at an affordable range. The optimum IATMD systems are installed on top of linear and nonlinear single-degree-of-freedom systems to mitigate their dynamic responses of them. The linear dynamic responses are determined through transfer matrix formations, and nonlinear dynamic responses are derived using the harmonic balance (HB) method. H_2 optimized IATMD is significantly 44.78% and 48.62% superior to the H_2 optimized conventional tuned mass damper one (CTMD1) and conventional tuned mass damper two (CTMD2). Furthermore, H_∞ optimized IATMD is significantly 39.98% superior to the H_∞ optimized conventional tuned mass damper (CTMD). According to the nonlinear dynamic analysis, H_2 optimized IATMD systems are significantly 35.33%, 76.97%, and 35.33% superior to the H_2 optimized CTMD. Furthermore, H_∞ optimized IATMD systems are significantly 25.92%, 73.64%, and 25.92% superior to the H_∞ optimized CTMD. The results of this study are mathematically accurate and feasible for practical applications.

Keywords: Inertial amplifier tuned mass dampers (IATMD); conventional tuned mass damper (CTMD); H_2 optimization; closed-form expressions; dynamic response reduction capacity; nonlinear dynamic analysis.

*Corresponding author.

1. Introduction

In order to mitigate the dynamic responses of the structures from natural calamities like earthquakes and cyclones, passive vibration control devices are implemented. Tuned mass dampers (TMDs) are one of these devices that assist in preventing vibrations. In 1909, Frahm was the first to patent the theory of TMD without addressing damping in TMD [Frahm, 1909]. When the natural frequency of the TMD is close to the excitation frequency, it is highly effective, but when the excitation frequency deviates from the natural frequency, there is no vibration reduction.

Ormondroyd and Den Hartog later addressed this drawback by integrating damped TMD and establishing closed-form expressions for the optimal design parameters [Ormondroyd, 1928]. This optimization method is referred to as the H_∞ optimization method, and its name is the fixed-point theory [Chen and Hu, 2019; Sun *et al.*, 2019]. When the controlled structure is subjected to harmonic excitation, this method is appropriate. Den Hartog authored a book containing a comprehensive illustration of this method [Den Hartog, 1985]. Ever since that period, comprehensive research has been conducted on TMD, and it has been implemented in a wide range of mechanical and civil applications [Zhang and Li, 2001; Lu *et al.*, 2020], such as car suspension systems, offshore platforms, buildings and bridges [Adhikari and Bhattacharya, 2012; Batou and Adhikari, 2019; Kasinos *et al.*, 2021]. When the controlled structure is subjected to white-noise random excitation, another method known as H_2 optimization is also employed to determine the optimal design parameters [Palmeri and Lombardo, 2011; Khodaparast *et al.*, 2008; Adhikari *et al.*, 2016]. Previous research has shown that the ability of a TMD to stop vibrations grows as its mass increases.

Smith has recently introduced a mechanical system called an inerter [Smith, 2020], which contradicts the conventional analogy for mitigating the vibration responses of structures. This inerter has been induced within or parallel to traditional passive vibration control devices in order to increase its energy dissipation capacity by amplifying the large effective mass through rotating mass using motion transformers within the system [Pietrosanti *et al.*, 2017]. A lot of these inerters have been used to improve the performance of machinery and parts in the field of mechanical engineering, especially in the suspension systems of cars and trains. Researchers have used inerter in civil engineering structures after seeing how well it worked in mechanical engineering [De Domenico *et al.*, 2019]. So far, many researchers have had satisfactory accuracy. Particularly, inerters have been put into the classical tuned mass damper and base isolator to control how buildings, wind turbines, and bridges respond to vibrations. In this paper, TMDs will be the primary topic [Petrini *et al.*, 2020; Wagg, 2021]. Most inerter-based TMDs, on the other hand, have been made with a flywheel-gear inerter. Apart from the flywheel-based inerter, there are also inertial amplifiers that have already achieved significant mass amplification and a large wide-bandgap at low frequencies. Because of these properties, inertial amplifiers can be used in construction to reduce vibration [Banerjee *et al.*, 2019, 2021; Adhikari and Banerjee, 2021]. However, the use of inertial amplifiers in finished constructions like buildings and bridges is rather limited. The majority of investigations, according to the present evaluation of the literature, were based on structural members such as beams and columns [Chowdhury *et al.*, 2021]. The inertial amplifier mechanism-tuned mass damper, whose structural typologies are comparable to inertial amplifiers, was recently explored by Cheng *et al.* However, they did not research any inertial amplifier-based TMDs and did not apply them to the nonlinear dynamic systems for vibration mitigation. Thus, a research scope has been detected.

Therefore, to address these research scopes, the inertial amplifier tuned mass dampers (IATMDs) for nonlinear dynamic systems to mitigate their dynamic responses are introduced in this paper. In addition, the exact-closed form expressions for optimal design parameters of IATMD in simplified form have been introduced in this paper using H_2 and H_∞ optimization methods [Chowdhury and Banerjee, 2022; Chowdhury *et al.*, 2022]. Applying these newly derived optimal closed-form solutions for the design parameters to IATMD, robust vibration reduction capacity has been achieved. Thus, the optimum IATMD is applied to the linear and nonlinear dynamic systems individually to mathematically determine the exact vibration reduction capacity of the optimum IATMD. The vibration reduction capacity of optimum IATMD has been compared to the vibration reduction capacity of conventional tuned mass dampers (CTMDs).

2. Structural Model and Equations of Motion

The schematic diagram of a single-degree-of-freedom system equipped with IATMD has been shown in Fig. 1(a). The schematic diagram of inertial amplifier and the corresponding free-body diagrams are shown in Figs. 1(b)–1(d).

m_d, k_d, and c_d refer to the static mass of IATMD. m_a and θ refer to the static mass and inertial angle of inertial amplifier. m_s, k_s, and c_s refer to the mass, stiffness, and damping of the primary structure. $\ddot{x}_g$ refers to the base excitation. u_s and u_d refer to the absolute dynamic responses of the primary structure and IATMD. x_a and y_a refer to the dynamic responses of inertial amplifier in x- and y-directions. Hence, the dynamic responses of the amplifier's masses in x- and y-directions are derived as

$$x_a = \frac{u_d + u_s}{2} \quad \text{and} \quad y_a = \pm\frac{u_d - u_s}{2\tan\theta} \tag{1}$$

The inertial forces generated through amplifier's mass have been derived as

$$f_x = m_a\ddot{x}_a \quad \text{and} \quad f_y = m_a\ddot{y}_a \tag{2}$$

The forces generated through rigid links are derived as

$$f_1 = \frac{1}{2}\left(\frac{f_y}{\sin\theta} - \frac{f_x}{\cos\theta}\right) \quad \text{and} \quad f_2 = \frac{1}{2}\left(\frac{f_y}{\sin\theta} + \frac{f_x}{\cos\theta}\right). \tag{3}$$

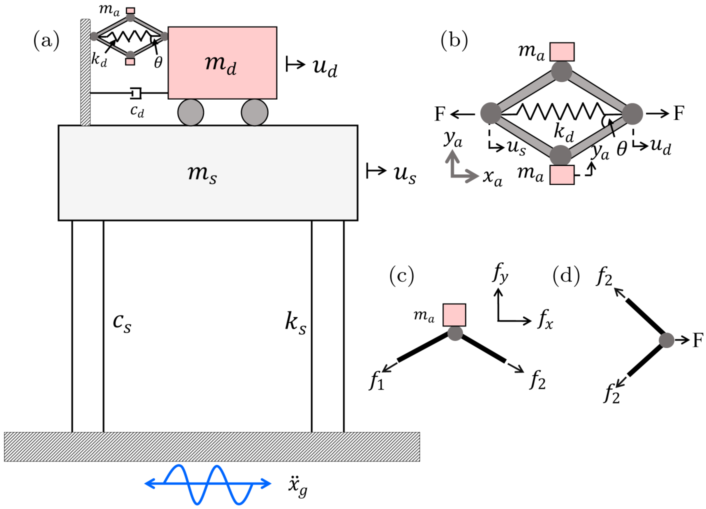

Fig. 1. The schematic diagram of (a) structure with IATMD, (b) inertial amplifier, and (c) (d) free-body diagrams.

The resultant force developed at the lateral terminals of the inertial amplifier has been derived as

$$\begin{aligned} F &= 2f_2\cos\theta + k_d(u_d - u_s) \\ &= \underbrace{\frac{0.5m_a}{\tan^2\theta}}_{c_1}(\ddot{u}_d - \ddot{u}_s) + \underbrace{0.5m_a}_{c_2}(\ddot{u}_s + \ddot{u}_d) + k_{ad}(u_d - u_s), \end{aligned} \tag{4}$$

where $c_1 = (0.5m_a/\tan^2\theta)$ and $c_2 = 0.5m_a$ are added with the static mass of the IATMD m_d. Therefore, the effective mass of IATMD has been derived as

$$m_{ad} = m_d + 0.5m_a\left(1 + \frac{1}{\tan^2\theta}\right) \tag{5}$$

The effective stiffness and damping of IATMD are derived as

$$k_{ad} = m_{ad}\omega_d^2 \quad \text{and} \quad c_{ad} = 2\zeta_d m_{ad}\omega_d \tag{6}$$

Newton's second law applies to derive the equations of motion for a single-degree-of-freedom system equipped with IATMDs after considering all the effective system parameters, such as effective mass stiffness and damping of the IATMD and expressed as

$$\begin{aligned} m_s\ddot{x}_s + c_s\dot{x}_s + k_s x_s - k_{ad}x_d - c_{ad}\dot{x}_d &= -m_s\ddot{x}_g, \\ m_{ad}\ddot{x}_d + m_{ad}\ddot{x}_s + k_{ad}x_d + c_{ad}\dot{x}_d &= -m_{ad}\ddot{x}_g. \end{aligned} \tag{7}$$

The controlled dynamic system is subjected to harmonic base excitation. Therefore, the steady-state solutions are considered $x_s = X_s e^{\mathrm{i}\omega t}$, $x_d = X_d e^{\mathrm{i}\omega t}$, and $\ddot{x}_g =$

$A_g e^{\mathrm{i}\omega t}$. Hence, the transfer function has been derived as

$$\begin{bmatrix} 2\,q\zeta_d\,\omega_d\mu_{ad} + q^2\mu_{ad} + {\omega_d}^2\mu_{ad} & q^2\mu_{ad} \\ -2\,q\zeta_d\,\omega_d\mu_{ad} - {\omega_d}^2\mu_{ad} & 2\,\zeta_s\,\omega_s\,q + q^2 + {\omega_s}^2 \end{bmatrix} \begin{Bmatrix} X_d \\ X_s \end{Bmatrix} = -\begin{bmatrix} \mu_{ad} \\ 1 \end{bmatrix} A_g. \quad (8)$$

The dynamic response of IATMD has been derived as

$$H_d = \frac{X_d}{A_g} = \frac{-\omega_s(2\,q\zeta_s + \omega_s)}{\Delta}. \quad (9)$$

The dynamic response of primary structure has been derived as

$$H_s = \frac{X_s}{A_g} = \frac{-2\,q\zeta_d\,\omega_d\mu_{ad} - 2\,\zeta_d\,\omega_d q - {\omega_d}^2\mu_{ad} - q^2 - {\omega_d}^2}{\Delta} \quad (10)$$

Δ has been derived as

$$\begin{aligned} \Delta = \quad & q^4 + (2\,\zeta_d\,\omega_d\mu_{ad} + 2\,\zeta_d\,\omega_d + 2\,\zeta_s\,\omega_s)q^3 \\ & + (4\,\zeta_d\,\zeta_s\,\omega_s\,\omega_d + {\omega_d}^2\mu_{ad} + {\omega_s}^2 + {\omega_d}^2)q^2 \\ & + (2\,\zeta_d\,{\omega_s}^2\omega_d + 2\,\zeta_s\,\omega_s\,{\omega_d}^2)q + {\omega_s}^2{\omega_d}^2. \end{aligned} \quad (11)$$

The effective mass ratio for IATMD has been derived as

$$\mu_e = \frac{\mu_{ad}}{\mu_d + 2\mu_a} = \frac{\mu_d}{\mu_d + 2\mu_a} + 0.5\frac{\mu_a}{\mu_d + 2\mu_a}\left(1 + \frac{1}{\tan^2\theta}\right). \quad (12)$$

$\mu_{ad} = m_{ad}/m_s$, $\mu_d = m_d/m_s$, and $\mu_a = m_a/m_s$ refer to the effective, damper, and amplifier mass ratios of IATMD. The contour diagram of effective mass ratio as a function of amplifier mass ratio and damper mass ratio of IATMD has been shown in Fig. 2(a). The inertial angle is considered $\theta = 10°$. The effective mass ratio increases when the damper mass and amplifier's mass ratio increases. The contour diagram of effective stiffness ratio as a function of amplifier mass ratio and damper mass ratio of IATMD has been shown in Fig. 2(b). The effective stiffness ratio increases

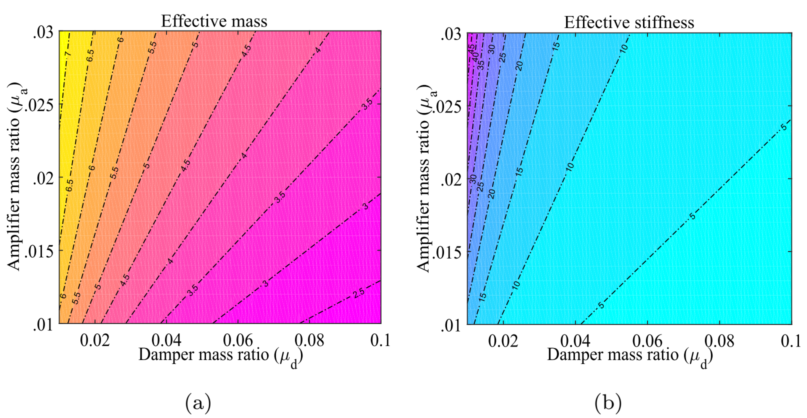

Fig. 2. The contour diagrams of (a) effective mass ratio and (b) effective stiffness ratio as a function of amplifier mass ratio and damper mass ratio of IATMD.

when the damper mass and amplifier's mass ratio increases. The effective stiffness ratio for IATMD has been derived as

$$\kappa_e = \frac{k_{ad}}{k_d} = \frac{\mu_{ad}\omega_d^2}{\mu_d\omega_d^2} = 1 + 0.5\frac{\mu_a}{\mu_d}\left(1 + \frac{1}{\tan^2\theta}\right). \tag{13}$$

3. H_2 Optimization

H_2 optimization has been performed to minimize the standard deviation of dynamic response of the controlled structures subjected to random-white noise excitations. The mathematical expressions for deriving standard deviations are determined as

$$\sigma^2_{x_{s,d}} = \int_{-\infty}^{\infty} \frac{\varepsilon_n(\omega)\,\mathrm{d}\omega}{\varrho_n(\mathrm{i}\omega)\varrho_n^*(\mathrm{i}\omega)} = \frac{\pi}{u_4}\frac{\det[\mathbf{A}_4]}{\det[\mathbf{B}_4]}, \tag{14}$$

$$A_4 = \begin{bmatrix} v_3 & b_2 & v_1 & v_0 \\ -u_4 & u_2 & -u_0 & 0 \\ 0 & -u_3 & u_1 & 0 \\ 0 & u_4 & -u_2 & u_0 \end{bmatrix} \quad \text{and} \quad B_4 = \begin{bmatrix} u_3 & -u_1 & 0 & 0 \\ -u_4 & u_2 & -u_0 & 0 \\ 0 & -u_3 & u_1 & 0 \\ 0 & u_4 & -u_2 & u_0 \end{bmatrix}. \tag{15}$$

Hence, the standard deviation of dynamic response of primary structure has been derived as

$$\sigma^2_{x_s} = \frac{S_0\pi\begin{pmatrix} 4\,{\omega_s}^2{\omega_d}^2{\mu_{ad}}^3{\zeta_d}^2 + 12\,{\omega_s}^2{\omega_d}^2{\mu_{ad}}^2{\zeta_d}^2 + {\mu_{ad}}^4{\omega_d}^4 \\ +\,12\,{\omega_s}^2{\omega_d}^2\mu_{ad}{\zeta_d}^2 + {\omega_s}^2{\omega_d}^2{\mu_{ad}}^3 + 4\,{\mu_{ad}}^3{\omega_d}^4 \\ +\,4\,{\omega_s}^2{\omega_d}^2{\zeta_d}^2 + 6\,{\mu_{ad}}^2{\omega_d}^4 - 3\,{\omega_s}^2{\omega_d}^2\mu_{ad} \\ +\,4\,\mu_{ad}{\omega_d}^4 + {\omega_s}^4 - 2\,{\omega_s}^2{\omega_d}^2 + {\omega_d}^4 \end{pmatrix}}{2\,\zeta_d\,\omega_d{\omega_s}^6\mu_{ad}}. \tag{16}$$

The mathematical formulations for derivations of optimal design parameters are listed as follows.

$$\frac{\partial\sigma^2_{x_s}}{\partial\zeta_d} = 0 \quad \text{and} \quad \frac{\partial\sigma^2_{x_s}}{\partial\omega_d} = 0. \tag{17}$$

Equation (16) is inserted into the first equation of Eq. (17). Therefore, the viscous damping ratio of IATMD has been derived as

$$\zeta_d = \frac{1}{2}\sqrt{\frac{(\mu_{ad}+1)^4{\omega_d}^4 + {\omega_s}^2(\mu_{ad}-2)(\mu_{ad}+1)^2{\omega_d}^2 + {\omega_s}^4}{{\omega_s}^2{\omega_d}^2(\mu_{ad}+1)^3}}. \tag{18}$$

Equation (18) is substituted into Eq. (16) and the modified SD of primary structure is derived as

$$\sigma^2_{x_s} = \frac{2\,S_0\pi\left((\mu_{ad}+1)^4{\omega_d}^4 + {\omega_s}^2(\mu_{ad}-2)(\mu_{ad}+1)^2{\omega_d}^2 + {\omega_s}^4\right)}{\sqrt{\frac{(\mu_{ad}+1)^4{\omega_d}^4 + {\omega_s}^2(\mu_{ad}-2)(\mu_{ad}+1)^2{\omega_d}^2 + {\omega_s}^4}{{\omega_s}^2{\omega_d}^2(\mu_{ad}+1)^3}}\,\omega_d{\omega_s}^6\mu_{ad}}. \tag{19}$$

Equation (19) is inserted in the second equation of Eq. (17). Hence, the optimal frequency for IATMD has been derived as

$$(\omega_d)_{\text{opt}} = \frac{\sqrt{4 - 2\,\mu_{ad}}\omega_s}{2(\mu_{ad} + 1)} \quad \text{and} \quad (\eta_d)_{\text{opt}} = \frac{\sqrt{4 - 2\,\mu_{ad}}}{2\,(\mu_{ad} + 1)}. \tag{20}$$

Equation (20) is substituted into Eq. 18. Hence, the optimal viscous damping ratio for IATMD has been derived as

$$(\zeta_d)_{\text{opt}} = \frac{\sqrt{2}\sqrt{\frac{(\mu_{ad}-4)\mu_{ad}}{(\mu_{ad}+1)(\mu_{ad}-2)}}}{4}. \tag{21}$$

The variations of optimal frequency ratio versus damper mass ratio for different values of inertial angle of IATMD have been shown in Fig. 3(a). The optimal frequency ratio decreases as the damper mass ratio increases and increases as the inertial angle increases. The variations of optimal frequency ratio versus damper mass ratio for different values of amplifier mass ratio of IATMD have been shown in Fig. 3(b). The optimal frequency ratio decreases as the amplifier mass ratio increases. Therefore, a higher damper mass ratio, a higher amplifier mass ratio, and a lower inertial angle achieve optimum IATMD with a lower frequency ratio. The variations of optimal viscous damping ratio versus damper mass ratio for different values of inertial angle of IATMD have been shown in Fig. 4(a). The optimal viscous damping ratio increases as the damper mass ratio increases and decreases as the inertial angle increases. The variations of optimal viscous damping ratio versus damper mass ratio for different values of amplifier mass ratio of IATMD have been shown in Fig. 4(b). The optimal viscous damping ratio increases as the amplifier mass ratio increases. For tuned mass dampers and a moderate viscous damping ratio with lower frequencies are recommended for achieving optimum vibration reduction capacity. Therefore, a higher damper mass ratio, a higher amplifier mass ratio, and a lower inertial angle achieve optimum IATMD with a moderate viscous damping ratio.

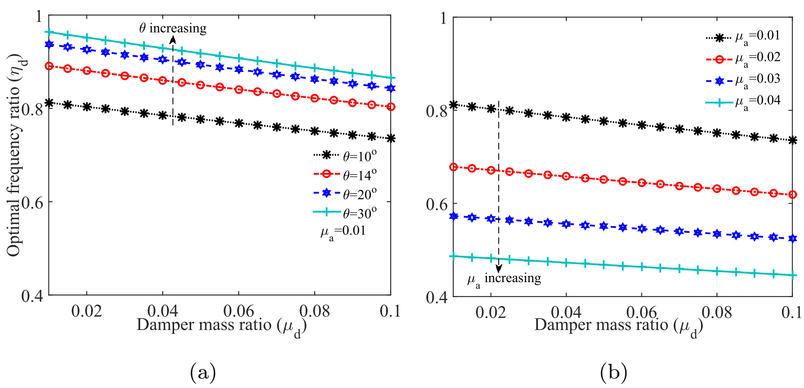

Fig. 3. The variations of optimal frequency ratio versus damper mass ratio for different values of (a) inertial angle and (b) amplifier's mass ratio of IATMD.

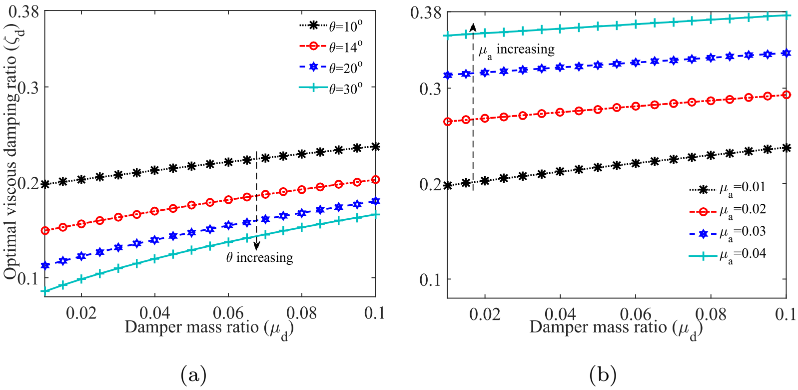

Fig. 4. The variations of optimal viscous damping ratio versus damper mass ratio for different values of (a) inertial angle and (b) amplifier's mass ratio of IATMD.

4. H_∞ Optimization

H_∞ optimization method has been applied to minimize the maximum dynamic responses of the controlled structures subjected to harmonic excitations. Hence, to perform that Eq. (8) has been re-written as

$$\begin{bmatrix} \mu_{ad}(2\,i\eta\,\zeta_d\,\eta_d - \eta^2 + {\eta_d}^2) & -\eta^2\mu_{ad} \\ -\eta_d\mu_{ad}(2\,i\eta\,\zeta_d + \eta_d) & -\eta^2 + 1 + 2\,i\zeta_s\,\eta \end{bmatrix} \begin{Bmatrix} X_d \\ X_s \end{Bmatrix} = -\begin{bmatrix} \mu_{ad} \\ 1 \end{bmatrix} \frac{A_g}{\omega_s^2}. \tag{22}$$

The dynamic response of IATMD has been derived as

$$H_d = \frac{X_d}{A_g}\omega_s^2 = \frac{2\mathrm{i}\zeta_s\,\eta + 1}{\Delta}. \tag{23}$$

The dynamic response of primary structure has been derived as

$$H_s = \frac{X_s}{A_g}\omega_s^2 = \frac{{\eta_d}^2\mu_{ad} - \eta^2 + {\eta_d}^2 + 2\,\mathrm{i}\eta\,\zeta_d\,\eta_d(\mu_{ad} + 1)}{\Delta} \tag{24}$$

Δ has been derived as

$$\begin{aligned}\Delta &= 4\,\eta^2\zeta_d\,\zeta_s\,\eta_d + \eta^2{\eta_d}^2\mu_{ad} - \eta^4 + \eta^2{\eta_d}^2 + \eta^2 - {\eta_d}^2 \\ &\quad + \mathrm{i}(2\,\eta^3\zeta_d\,\eta_d\mu_{ad} + 2\,\eta^3\zeta_d\,\eta_d + 2\,\eta^3\zeta_s - 2\,\eta\,\zeta_s\,{\eta_d}^2 - 2\,\eta\,\zeta_d\,\eta_d)\end{aligned} \tag{25}$$

The resultant of H_s has been written as

$$|H_s| = \sqrt{\frac{x_1^2 + \zeta_d^2 x_2^2}{x_3^2 + \zeta_d^2 x_4^2}} = \frac{x_2}{x_4}\sqrt{\frac{\frac{x_1^2}{x_2^2} + \zeta_d^2}{\frac{x_3^2}{x_4^2} + \zeta_d^2}} \tag{26}$$

From Eq. (26), the first constraint [Den Hartog, 1985] has been derived as

$$\left|\frac{x_1}{x_2}\right| = \left|\frac{x_3}{x_4}\right| \tag{27}$$

An equation has been derived from Eq. (27) and expressed as

$$\begin{aligned}(2\,\mu_{ad}+2)\eta^4 + 2\,{\eta_d}^2\mu_{ad} + 2\,{\eta_d}^2 \\ + (-2\,{\eta_d}^2{\mu_{ad}}^2 - 4\,{\eta_d}^2\mu_{ad} - 2\,{\eta_d}^2 - \mu_{ad} - 2)\eta^2 = 0\end{aligned} \tag{28}$$

$$\eta_1^2+\eta_2^2 = \frac{({\eta_d}^2{\mu_{ad}}^2 + 2\,{\eta_d}^2\mu_{ad} + {\eta_d}^2 + (\mu_{ad}/2) + 1)}{(\mu_{ad}+1)} \tag{29}$$

From Eq. (26), the second constraint [Den Hartog, 1985] has been derived as

$$(H_s)_{\eta_1,\eta_2} = \left|\frac{x_2}{x_4}\right| \quad \text{and} \quad (H_s)_{\eta_1,\eta_2} = \frac{1+\mu_{ad}}{|1-\eta_{1,2}^2(1+\mu_{ad})|} \tag{30}$$

$$\eta_1^2+\eta_2^2 = \frac{2}{1+\mu_{ad}} \tag{31}$$

Equations (29) and (31) are equated to derive the closed-form expression for optimal frequency ratio of IATMD and expressed as

$$(\eta_d)_{\text{opt}} = \frac{\sqrt{1-0.5\mu_{ad}}}{1+\mu_{ad}} \tag{32}$$

The optimum $\eta_{1,2}$, H_s, and ζ_d has also been derived in a similar manner and expressed as

$$(\eta_{1,2})_{\text{opt}} = \frac{\sqrt{1\pm\sqrt{0.5\mu_{ad}}}}{1+\mu_{ad}} \tag{33}$$

The optimal dynamic response of IATMD has been derived as

$$(H_s)_{\text{opt}} = \frac{1+\mu_{ad}}{\sqrt{0.5\mu_{ad}}} \tag{34}$$

The exact closed-form expression for optimal viscous damping ratio of IATMD has been derived as

$$(\zeta_d)_{\text{opt}} = \sqrt{\frac{\mu_{ad}(3-\sqrt{0.5\mu_{ad}})}{8(1+\mu_{ad})(1-0.5\mu_{ad})}} \tag{35}$$

The variations of optimal frequency ratio versus damper mass ratio for different values of inertial angle of IATMD have been shown in Fig. 5(a). The optimal frequency ratio decreases as the damper mass ratio increases and increases as the inertial angle increases. The variations of optimal frequency ratio versus damper mass ratio for different values of amplifier mass ratio of IATMD have been shown in Fig. 5(b). The optimal frequency ratio decreases as the amplifier mass ratio increases. Therefore, a higher damper mass ratio, a higher amplifier mass ratio, and a lower inertial angle achieve optimum IATMD with a lower frequency ratio. The variations of optimal viscous damping ratio versus damper mass ratio for different values of inertial angle of IATMD have been shown in Fig. 6(a). The optimal viscous damping ratio increases as the damper mass ratio increases and decreases as the inertial angle increases.The variations of optimal viscous damping ratio versus damper mass ratio

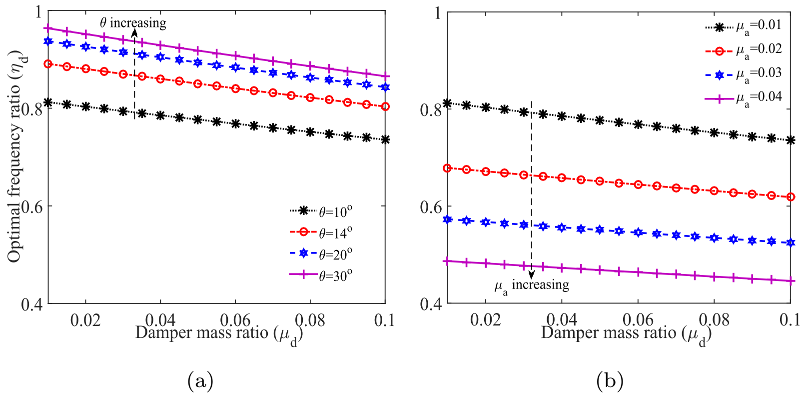

Fig. 5. The variations of optimal frequency ratio versus damper mass ratio for different values of (a) inertial angle and (b) amplifier's mass ratio of IATMD.

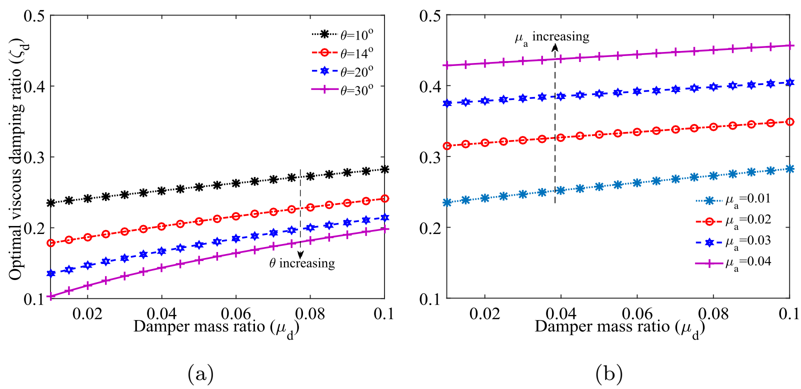

Fig. 6. The variations of optimal viscous damping ratio versus damper mass ratio for different values of (a) inertial angle and (b) amplifier's mass ratio of IATMD.

for different values of amplifier mass ratio of IATMD have been shown in Fig. 6(b). The optimal viscous damping ratio increases as the amplifier mass ratio increases. For tuned mass dampers, a moderate viscous damping ratios with lower frequencies are recommended for achieving optimum vibration reduction capacity. Therefore, a higher damper mass ratio, a higher amplifier mass ratio, and a lower inertial angle achieve optimum IATMD with a moderate viscous damping ratio.

5. Robustness of H_2 and H_∞ Optimized IATMD

The variations of optimal dynamic responses of primary structures controlled by H_2 optimized IATMD versus frequency ratio for different values of viscous damping ratio have been shown in Fig. 7(a). The primary structure's viscous damping is considered $\zeta_s = 0.00$. For $\zeta_d = 0$, the controlled structures are vibrating at their

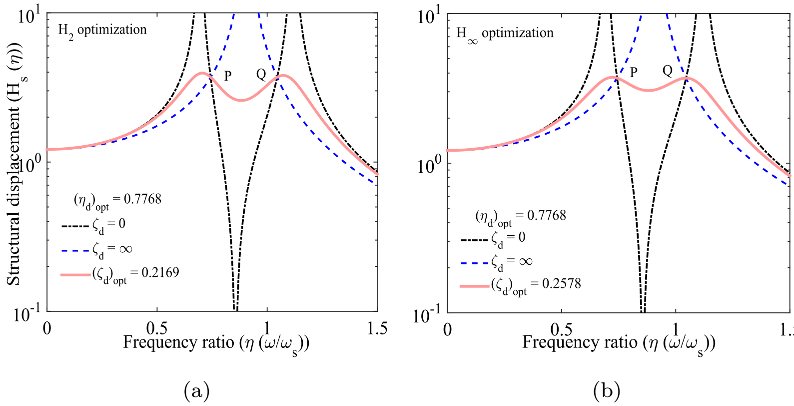

Fig. 7. The variations of optimal dynamic responses of primary structures controlled by (a) H_2 and (b) H_∞ optimized IATMD versus frequency ratio for different values of viscous damping ratio.

Eigen frequencies, i.e., $\eta = 0.6943, 1.119$. The anti-resonance frequency point is located at $\eta = 0.8566$. For $\zeta_d > 0$, the controlled structures are vibrating at their resonating frequencies, i.e., $\eta = 0.6983, 1.081$. The minima frequency point located at $\eta = 0.8763$. At $\zeta_d = \infty$, the maximum peaks of controlled structures are merged into one, i.e., SDOF and frequency peak is located at $\eta = 0.9072$. The variations of optimal dynamic responses of primary structures controlled by H_∞ optimized IATMD versus frequency ratio for different values of viscous damping ratio have been shown in Fig. 7(b). The primary structure's viscous damping is considered $\zeta_s = 0.00$. For $\zeta_d = 0$, the controlled structures are vibrating at their Eigen frequencies, i.e., $\eta = 0.6944, 1.119$. The anti-resonance frequency point is located at $\eta = 0.8566$. For $\zeta_d > 0$, the controlled structures are vibrating at their resonating frequencies, i.e., $\eta = 0.7223, 1.046$. The minima frequency point is located at $\eta = 0.8803$. At $\zeta_d = \infty$, the maximum peaks of controlled structures are merged into one, i.e., SDOF and frequency peak is located at $\eta = 0.9069$.

The variations of optimal dynamic responses of primary structures controlled by H_2 optimized IATMD and conventional tuned mass dampers (CTMD) versus frequency ratio have been shown in Fig. 8(a). The details of design parameters for these graphs are listed in Table 1. The maximum dynamic response of the uncontrolled structure has been determined as 50. The maximum dynamic response of the structure controlled by conventional tuned mass damper 1 (CTMD1) [Warburton, 1982; Zilletti *et al.*, 2012] and conventional tuned mass damper 2 (CTMD2) [Iwata, 1982] has been determined as 7.0968 and 7.6271. The maximum dynamic response of the structure controlled by IATMD has been determined as 3.9188. Therefore, the dynamic response capacity of H_2 optimized IATMD is significantly 44.78% and 48.62% superior to the H_2 optimized CTMD1 and CTMD2. The variations of optimal dynamic responses of primary structures controlled by H_∞ optimized IATMD and CTMD versus frequency ratio have been shown in Fig. 8(b). The details of

Table 1. The optimal design parameters of uncontrolled and controlled structures. Equations (20) and (21) are applied for H_2 optimized mass dampers.

Symbols			H_2 optimization		
CTMD1	CTMD2	IATMD	CTMD1	CTMD2	IATMD
ζ_s	ζ_s	ζ_s	0.01	0.01	0.01
ζ_d	ζ_d	ζ_d	0.1198	0.1225	0.2124
η_d	η_d	η_d	0.9574	0.9713	0.7855
μ_d	μ_d	$\mu_d + 2\mu_a$	0.06	0.06	0.06
μ_d	μ_d	μ_d	0.06	0.06	0.04
...	...	μ_a	...	...	0.01
...	...	θ	...	...	10°

Note: CTMD1 = Warburton [1982] and Zilletti *et al.* [2012].
CTMD2 = Iwata [1982].

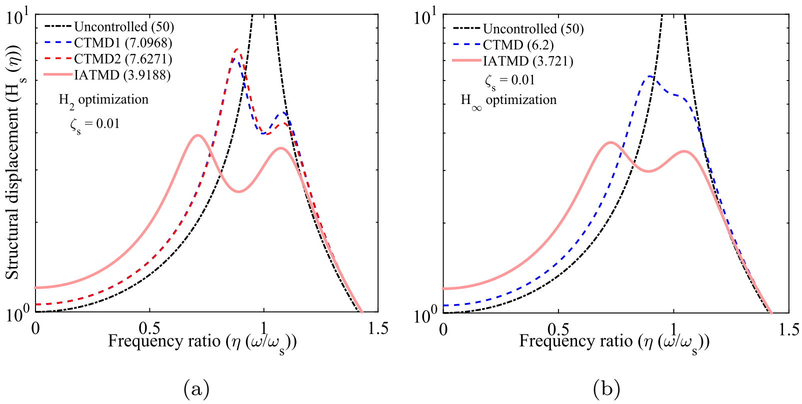

Fig. 8. The variations of optimal dynamic responses of primary structures controlled by (a) H_2 and (b) H_∞ optimized IATMD and CTMD versus frequency ratio.

Table 2. The optimal design parameters of uncontrolled and controlled structures. Equations (32) and (35) are applied for H_∞ optimized mass dampers.

Symbols		H_∞ optimization	
CTMD	IATMD	CTMD	IATMD
ζ_s	ζ_s	0.01	0.01
ζ_d	ζ_d	0.1682	0.2524
η_d	η_d	0.9434	0.7855
μ_d	$\mu_d + 2\mu_a$	0.06	0.06
μ_d	μ_d	0.06	0.04
...	μ_a	...	0.01
...	θ	...	10°

Note: CTMD = Krenk [2005], Den Hartog and Ormondroyd [1928] and Nishihara and Asami [2002].

design parameters for these graphs are listed in Table 2. The maximum dynamic response of the uncontrolled structure has been determined as 50. The maximum dynamic response of the structure controlled by CTMD [Krenk, 2005; Den Hartog and Ormondroyd, 1928; Nishihara and Asami, 2002] has been determined as 6.2. The maximum dynamic response of the structure controlled by IATMD has been determined as 3.721. Therefore, the dynamic response capacity of H_∞ optimized IATMD is significantly 39.98% superior to the H_∞ optimized CTMD.

6. Nonlinear Dynamic Analysis

IATMD has been installed on the nonlinear dynamic system, and the corresponding schematic diagram has been displayed in Fig. 9. Newton's second law applies to derive the equations of motion for a nonlinear dynamic system equipped with IATMDs after considering all the effective system parameters, such as effective mass stiffness and damping of the IATMD and the equations are expressed as

$$\begin{gathered} m_s\ddot{u}_s + c_s\dot{u}_s + k_{s1}u_s + k_{s2}u_s^3 - k_{ad}x_d - c_{ad}\dot{x}_d = F\cos\omega t \\ m_{ad}\ddot{x}_d + m_{ad}\ddot{u}_s + k_{ad}x_d + c_{ad}\dot{x}_d = 0 \end{gathered} \tag{36}$$

The controlled structure is subjected to harmonic excitation. Therefore, the harmonic balance (HB) method has been applied to derive the dynamic responses of the controlled structures analytically. The steady-state solutions are considered

$$x_d = X_d\cos(\omega t + \beta) \quad \text{and} \quad u_s = U_s\cos(\omega t + \alpha) \tag{37}$$

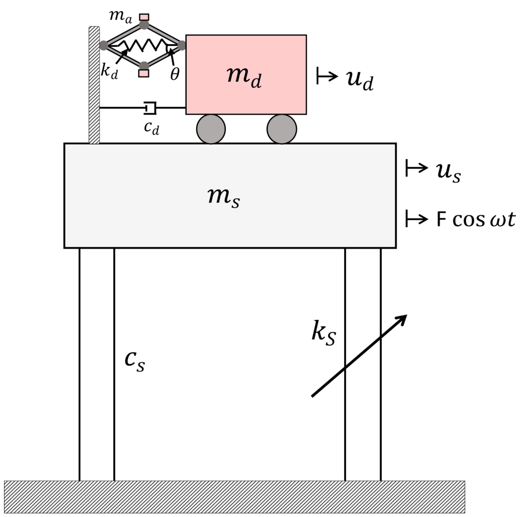

Fig. 9. The schematic diagram of IATMD equipped with nonlinear dynamic system.

Equation (37) has been substituted in the second equation of Eq. (36). Therefore, Eq. (36) has been modified as

$$-\mu_{ad}\begin{pmatrix} X_d(\omega^2-{\omega_d}^2)\cos(\omega\, t+\beta) \\ +2\,\sin(\omega\, t+\beta)X_d\omega_d\omega\,\zeta_d+U_s\omega^2\cos(\omega\, t+\alpha)\end{pmatrix}=0 \tag{38}$$

The trigonometric function has been derived as

$$\begin{aligned}\cos(\omega t+\alpha)&=\cos((\omega t+\beta)+(\alpha-\beta))\\ &=\cos(\omega t+\beta)\cos(\alpha-\beta)-\sin(\omega t+\beta)\sin(\alpha-\beta)\end{aligned} \tag{39}$$

Equation (38) has been re-written as

$$\begin{matrix} X_d(\omega^2-{\omega_d}^2)\cos(\omega\, t+\beta)+2\,\sin(\omega\, t+\beta)X_d\omega_d\omega\,\zeta_d \\ +U_s\omega^2\cos(\omega\, t+\beta)\cos(\alpha-\beta)-U_s\omega^2\sin(\omega\, t+\beta)\sin(\alpha-\beta)\end{matrix}=0 \tag{40}$$

After applying the HB, the trigonometric functions are derived as

$$\begin{aligned}&\cos(\alpha-\beta)=-\frac{X_d(\omega^2-{\omega_d}^2)}{\omega^2U_s}\quad\text{and}\quad \sin(\alpha-\beta)=\frac{2\zeta_d\,X_d\omega_d}{\omega\,U_s}\\ &\tan(\alpha-\beta)=\frac{2\omega\,\zeta_d\,\omega_d}{{\omega_d}^2-\omega^2}=\frac{2\eta\,\zeta_d\,\eta_d}{{\eta_d}^2-\eta^2}\end{aligned} \tag{41}$$

The closed-form expression for X_d has been derived using Eq. (41). Hence, the derivations are listed as follows.

$$\sin^2(\alpha-\beta)+\cos^2(\alpha-\beta)=\left(\frac{X_d(\omega^2-{\omega_d}^2)}{\omega^2U_s}\right)^2+\left(\frac{2\zeta_d\,X_d\omega_d}{\omega\,U_s}\right)^2 \tag{42}$$

The closed-form expression for dynamic response of IATMD has been derived as

$$X_d=\frac{U_s\omega^2}{\sqrt{4\,\omega^2{\zeta_d}^2{\omega_d}^2+\omega^4-2\,\omega^2{\omega_d}^2+{\omega_d}^4}} \tag{43}$$

The variations of phase angle differences versus frequency ratio of controlled structures for H_2 optimized IATMD have been shown in Fig. 10(a). The variations of phase angle differences versus frequency ratio of controlled structures for H_∞ optimized IATMD have been shown in Fig. 10(b). From both figures, it has been observed that the controlled structures are in phase condition at $\eta = 0.813$ and out-of-phase conditions are located at $\eta > 0.813$. Equation (37) has been substituted in the first equation of Equation (36). Therefore, the equation has been modified as

$$\begin{matrix} 1/4\,\gamma\,{\omega_s}^2{U_s}^3\cos(3\,\omega t+3\alpha) \\ +1/4\begin{pmatrix} 3\,\gamma\,{\omega_s}^2{U_s}^3+(-4\,\omega^2+4\,{\omega_s}^2)U_s \\ -8\,B\omega\,\zeta_d\,X_d\mu_{ad}\omega_d-4\,AX_d\mu_{ad}{\omega_d}^2-4\,Fw_1\end{pmatrix}\cos(\omega t+\alpha) \\ +2\,\sin(\omega t+\alpha)\begin{pmatrix} A\omega\,\zeta_d\,X_d\mu_{ad}\omega_d-1/2\,BX_d\mu_{ad}{\omega_d}^2 \\ -\zeta_s\,\omega_s\,U_s\omega-1/2\,Fw_2\end{pmatrix}\end{matrix}=0 \tag{44}$$

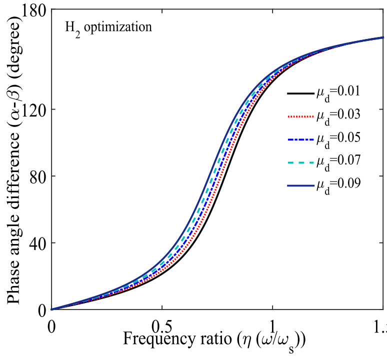

(a)

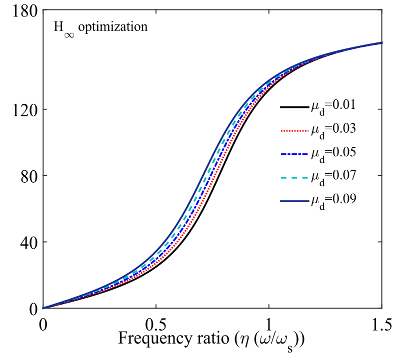

(b)

Fig. 10. The variations of phase angle differences versus frequency ratio of controlled structures for (a) H_2 and (b) H_∞ optimized IATMD.

where $A = \cos(\alpha - \beta)$, $B = \sin(\alpha - \beta)$, $w_1 = \cos\alpha$, $w_2 = \sin\alpha$. The HB method has been applied and the trigonometric functions are derived as

$$\cos\alpha = \frac{1}{F}\left(3/4\,\gamma\,{\omega_s}^2{U_s}^3 - (\omega^2 - {\omega_s}^2)U_s - \frac{\mu_{ad}{\omega_d}^2{X_d}^2(4\,\omega^2{\zeta_d}^2 - \omega^2 + {\omega_d}^2)}{\omega^2 U_s}\right) \quad (45)$$

$$\sin\alpha = -\frac{2\omega\,(\zeta_d\,{X_d}^2\mu_{ad}\omega_d + \zeta_s\,\omega_s\,{U_s}^2)}{U_s F} \quad (46)$$

Equations (45) and (46) have been written as

$$\sin^2\alpha + \cos^2\alpha = \left(\frac{2\omega\,(\zeta_d\,{X_d}^2\mu_{ad}\omega_d + \zeta_s\,\omega_s\,{U_s}^2)}{U_s F}\right)^2 + \left(\frac{1}{F}\left(3/4\,\gamma\,{\omega_s}^2{U_s}^3 - (\omega^2 - {\omega_s}^2)U_s - \frac{\mu_{ad}{\omega_d}^2{X_d}^2(4\,\omega^2{\zeta_d}^2 - \omega^2 + {\omega_d}^2)}{\omega^2 U_s}\right)\right)^2 \quad (47)$$

Equation 43 has been substituted in the first equation of Eq. 50. Therefore, the nonlinear dynamic response of the primary structure has been derived as

$$u_3{U_s}^6 + u_2{U_s}^4 + u_1U_s^2 + u_0 = 0$$

$$p_1 = U_{s1}^2 = \frac{\sqrt[3]{-108\,u_0{u_3}^2 + 36\,u_3u_2u_1 + 12\,\sqrt{3}V_1\,u_3 - 8\,{u_2}^3}}{6u_3} - \frac{2(3\,u_3u_1 - {u_2}^2)}{3u_3\sqrt[3]{-108\,u_0{u_3}^2 + 36\,u_3u_2u_1 + 12\,\sqrt{3}V_1\,u_3 - 8\,{u_2}^3}} - \frac{u_2}{3u_3} \quad (48)$$

$$p_2 = U_{s2}^2 = -\frac{\sqrt[3]{-108\,u_0{u_3}^2 + 36\,u_3u_2u_1 + 12\,\sqrt{3}V_1\,u_3 - 8\,{u_2}^3}}{12u_3} + \frac{3\,u_3u_1 - {u_2}^2}{3u_3\sqrt[3]{-108\,u_0{u_3}^2 + 36\,u_3u_2u_1 + 12\,\sqrt{3}V_1\,u_3 - 8\,{u_2}^3}} - \frac{u_2}{3u_3}$$

$$+\frac{1}{2}\left(\mathrm{i}\sqrt{3}\left(\frac{\sqrt[3]{-108\,u_0{u_3}^2+36\,u_3u_2u_1+12\,\sqrt{3}V_1\,u_3-8\,{u_2}^3}}{6u_3}+\frac{2(3\,u_3u_1-{u_2}^2)}{3u_3\sqrt[3]{-108\,u_0{u_3}^2+36\,u_3u_2u_1+12\,\sqrt{3}V_1\,u_3-8\,{u_2}^3}}\right)\right) \tag{49}$$

$$\begin{aligned} p_3=U_{s3}^2 &= -\frac{\sqrt[3]{-108\,u_0{u_3}^2+36\,u_3u_2u_1+12\,\sqrt{3}V_1\,u_3-8\,{u_2}^3}}{12u_3} \\ &\quad+\frac{3\,u_3u_1-{u_2}^2}{3u_3\sqrt[3]{-108\,u_0{u_3}^2+36\,u_3u_2u_1+12\,\sqrt{3}V_1\,u_3-8\,{u_2}^3}}-\frac{u_2}{3u_3} \\ &\quad-\frac{1}{2}\left(\mathrm{i}\sqrt{3}\left(\frac{\sqrt[3]{-108\,u_0{u_3}^2+36\,u_3u_2u_1+12\,\sqrt{3}V_1\,u_3-8\,{u_2}^3}}{6u_3}+\frac{2(3\,u_3u_1-{u_2}^2)}{3u_3\sqrt[3]{-108\,u_0{u_3}^2+36\,u_3u_2u_1+12\,\sqrt{3}V_1\,u_3-8\,{u_2}^3}}\right)\right) \end{aligned} \tag{50}$$

where

$$V_1=\sqrt{27\,{u_3}^2{u_0}^2-18\,u_3u_2u_1u_0+4\,u_3{u_1}^3+4\,{u_2}^3u_0-{u_2}^2{u_1}^2} \tag{51}$$

The closed-form expressions for u_3, u_2, u_1, and u_0 are derived as

$$\begin{aligned} u_3 &= 9\,{\omega_s}^4\gamma^2({\omega_d}^4+(4\,{\zeta_d}^2-2)\omega^2{\omega_d}^2+\omega^4)^2 \\ &\qquad -24\,({\omega_d}^4+(4\,{\zeta_d}^2-2)\omega^2{\omega_d}^2+\omega^4){\omega_s}^2\gamma \\ u_2 &= \begin{pmatrix}\omega^6+(((4\,\mu_{ad}+4){\zeta_d}^2-\mu_{ad}-2){\omega_d}^2-{\omega_{0s}}^2)\omega^4 \\ +((\mu_{ad}+1){\omega_d}^4+(-4\,{\zeta_d}^2+2){\omega_s}^2{\omega_d}^2)\omega^2-{\omega_s}^2{\omega_d}^4\end{pmatrix} \\ &\qquad (16\,{\omega_d}^4+16\,(4\,{\zeta_d}^2-2)\omega^2{\omega_d}^2+16\,\omega^4) \end{aligned} \tag{52}$$

$$u_1=\begin{pmatrix}\omega^8+\begin{pmatrix}4(-1/2+(\mu_{ad}+1){\zeta_d}^2)(\mu_{ad}+1){\omega_d}^2 \\ +8\,\zeta_d\,\zeta_s\,\omega_s\,\mu_{ad}\omega_d+(4\,{\zeta_s}^2-2){\omega_s}^2\end{pmatrix}\omega^6 \\ +\begin{pmatrix}(\mu_{ad}+1)^2{\omega_d}^4+{\omega_s}^4 \\ +16\,{\omega_s}^2\begin{pmatrix}({\zeta_s}^2-1/2\,\mu_{ad}-1/2){\zeta_d}^2 \\ -\,1/2\,{\zeta_s}^2+1/8\,\mu_{ad}+1/4\end{pmatrix}{\omega_d}^2\end{pmatrix}\omega^4 \\ +4(({\zeta_s}^2-1/2\,\mu_{ad}-1/2){\omega_d}^2+{\omega_s}^2({\zeta_d}^2-1/2)){\omega_s}^2{\omega_d}^2\omega^2 \\ +{\omega_s}^4{\omega_d}^4\end{pmatrix} \tag{53}$$

$$u_0=-16\,F^2({\omega_d}^4+(4\,{\zeta_d}^2-2)\omega^2{\omega_d}^2+\omega^4)^2 \tag{54}$$

The variations of optimal nonlinear dynamic responses of primary structures controlled by H_2 optimized IATMD and CTMDs versus frequency ratio have been shown in Fig. 11(a). The details of design parameters for these graphs are listed in

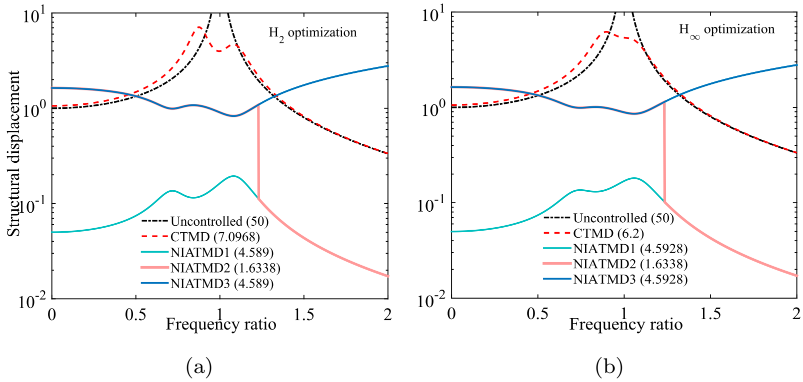

Fig. 11. The variations of optimal nonlinear dynamic responses of primary structures controlled by (a) H_2 and (b) H_∞ optimized CTMD and IATMD versus frequency ratio.

Table 3. The maximum dynamic response of the uncontrolled structure has been determined as 50. The maximum dynamic response of the structure controlled by CTMD [Warburton, 1982; Zilletti *et al.*, 2012] has been determined as 7.0968. Three analytical closed-form expressions for nonlinear dynamic responses of the primary structures have been derived. Equation (50) has been utilized to determine the nonlinear dynamic responses for primary structures controlled by H_2 optimized IATMD. The maximum nonlinear dynamic responses of the primary structures controlled by H_2 optimized IATMD have been evaluated as 4.589, 1.6338, 4.589. Therefore, H_2 optimized IATMD systems are significantly 35.33%, 76.97%, and 35.33% superior to the H_2 optimized CTMD. The variations of optimal dynamic responses of primary structures controlled by H_∞ optimized IATMD and CTMDs versus frequency ratio have been shown in Fig. 11(b). The details of design parameters for these graphs are listed in Table 4. The maximum dynamic response of the uncontrolled structure has been determined as 50. The maximum dynamic response of the structure controlled by CTMD [Krenk, 2005; Den Hartog and Ormondroyd, 1928; Nishihara and Asami, 2002] has been determined as 6.2. The maximum nonlinear dynamic responses of the primary structures controlled by H_∞ optimized IATMD have been evaluated as 4.5928, 1.6338, 4.5928. Therefore, H_∞ optimized IATMD systems are significantly 25.92%, 73.64%, and 25.92% superior to the H_∞ optimized CTMD.

7. Summary and Conclusions

The dynamic response reduction capacity of optimum IATMD has been determined in this study. H_2 and H_∞ optimization methods are applied to derive the closed-form expressions for optimal design parameters for IATMD. The HB method has been applied to derive the nonlinear dynamic responses of the controlled structures. The dynamic response reduction capacity of optimum IATMD has been compared

Table 3. The optimal design parameters of uncontrolled and controlled structures. Equations (20) and (21) are applied for H_2 optimized mass dampers.

Symbols		H_2 optimization	
CTMD	IATMD	CTMD	IATMD
ζ_s	ζ_s	0.01	0.01
ζ_d	ζ_d	0.1198	0.2124
η_d	η_d	0.9574	0.7855
μ_d	$\mu_d + 2\mu_a$	0.06	0.06
μ_d	μ_d	0.06	0.04
$\cdots$	μ_a	$\cdots$	0.10
$\cdots$	θ	$\cdots$	10°

Note: CTMD = Warburton [1982] and Zilletti *et al.* [2012].

Table 4. The optimal design parameters of uncontrolled and controlled structures. Equations (32) and (35) are applied for H_∞ optimized mass dampers.

Symbols		H_∞ optimization	
CTMD	IATMD	CTMD	IATMD
ζ_s	ζ_s	0.01	0.01
ζ_d	ζ_d	0.1682	0.2524
η_d	η_d	0.9434	0.7855
μ_d	$\mu_d + 2\mu_a$	0.06	0.06
μ_d	μ_d	0.06	0.04
$\cdots$	μ_a	$\cdots$	0.10
$\cdots$	θ	$\cdots$	10°

Note: CTMD = Krenk [2005], Den Hartog and Ormondroyd [1928] and Nishihara and Asami [2002].

with the dynamic response reduction capacity of CTMD. The significant outcomes of the study are listed as follows.

- A higher damper mass ratio, a higher amplifier mass ratio, and a lower inertial angle are recommended to achieve H_2 optimized IATMD with a moderate viscous damping and lower frequency ratios.
- For H_∞ optimized IATMD, a higher damper mass ratio, a higher amplifier mass ratio, and a lower inertial angle are also recommended.
- The dynamic response capacity of H_2 optimized IATMD is significantly 44.78% and 48.62% superior to the H_2 optimized CTMD1 and CTMD2.
- The dynamic response capacity of H_∞ optimized IATMD is significantly 39.98% superior to the H_∞ optimized CTMD.
- According to the nonlinear dynamic analysis, H_2 optimized IATMD systems are significantly 35.33%, 76.97%, and 35.33% superior to the H_2 optimized CTMD.
- Furthermore, H_∞ optimized IATMD systems are significantly 25.92%, 73.64%, and 25.92% superior to the H_∞ optimized CTMD.

The closed-form expressions for optimal design parameters of IATMD are one of the significant contributions of the paper. The experimental works considering this novel tuned mass dampers will be the future perspective of the research.

Acknowledgments

The authors' would like to acknowledge the Inspire faculty grant, Grant No. DST/INSPIRE/04/2018/000052 for partial financial support for the project. SC would like to acknowledge the MHRD grant received from IIT Delhi during the period of this research work.

References

Adhikari, S., Friswell, M., Litak, G. and Khodaparast, H. H. [2016] "Design and analysis of vibration energy harvesters based on peak response statistics," *Smart Materials and Structures* **25**(6), 065009.

Adhikari, S. and Banerjee, A. [2021] "Enhanced low-frequency vibration energy harvesting with inertial amplifiers," *Journal of Intelligent Material Systems and Structures* **33**, 822–838.

Adhikari, S. and Bhattacharya, S. [2012] "Dynamic analysis of wind turbine towers on flexible foundations," *Shock and Vibration* **19**(1), 37–56.

Banerjee, A., Das, R. and Calius, E. P. [2019] "Waves in structured mediums or metamaterials: A review," *Archives of Computational Methods in Engineering* **26**(4), 1029–1058.

Banerjee, A., Adhikari, S. and Hussein, M. I. [2021] "Inertial amplification band-gap generation by coupling a levered mass with a locally resonant mass," *International Journal of Mechanical Sciences* **207**, 106630.

Batou, A. and Adhikari, S. [2019] "Optimal parameters of viscoelastic tuned-mass dampers," *Journal of Sound and Vibration* **445**, 17–28.

Chen, M. Z. and Hu, Y. [2019] "Analysis for inerter-based vibration system," in *Inerter and its Application in Vibration Control Systems*, Springer, pp. 19–39.

Chowdhury, S., Banerjee, A. and Adhikari, S. [2022] "Optimal design of inertial amplifier base isolators for dynamic response control of multi-storey buildings," *International Journal of Structural Stability and Dynamics* 2350047.

Chowdhury, S., Banerjee, A. and Adhikari, S. [2021] "Enhanced seismic base isolation using inertial amplifiers," *Structures* **33**, 1340–1353.

Chowdhury, S., Banerjee, A. and Adhikari, S. [2022] "Optimal negative stiffness inertial-amplifier-base-isolators: Exact closed-form expressions," *International Journal of Mechanical Sciences* **218**, 107044.

Chowdhury, S. and Banerjee, A. [2022] "The exact closed-form expressions for optimal design parameters of resonating base isolators," *International Journal of Mechanical Sciences* **224**, 107284.

Den Hartog, J. and Ormondroyd, J. [1928] "Theory of the dynamic vibration absorber," *ASME Journal of Applied Mechanics* **50**(7), 11–22.

Den Hartog, J. P. [1985] *Mechanical Vibrations* (Courier Corporation).

De Domenico, D., Deastra, P., Ricciardi, G., Sims, N. D. and Wagg, D. J. [2019] "Novel fluid inerter based tuned mass dampers for optimised structural control of base-isolated buildings," *Journal of the Franklin Institute* **356**(14), 7626–7649.

Frahm, H. [1909] "Devices for damping vibration of bodies," US Patent 989958.
Iwata, Y. [1982] "On the construction of the dynamic vibration absorbers," *Japan Society of Mechanical Engineering* **820**(8), 150–152.
Kasinos, S., Palmeri, A., Lombardo, M. and Adhikari, S. [2021] "A reduced modal subspace approach for damped stochastic dynamic systems," *Computers and Structures* **257**, 106651.
Khodaparast, H. H., Mottershead, J. E. and Friswell, M. I. [2008] "Perturbation methods for the estimation of parameter variability in stochastic model updating," *Mechanical Systems and Signal Processing* **22**(8), 1751–1773.
Krenk, S. [2005] Frequency analysis of the tuned mass damper, *Journal of Applied Mechanics* **72** 936–942.
Lu, S., Jiang, Y., Zhang, W. and Song, X. [2020] "Vibration suppression of cantilevered piezoelectric laminated composite rectangular plate subjected to aerodynamic force in hygrothermal environment," *European Journal of Mechanics-A/Solids* **83**, 104002.
Nishihara, O. and Asami, T. [2002] "Closed-form solutions to the exact optimizations of dynamic vibration absorbers (minimizations of the maximum amplitude magnification factors)," *Journal of Vibration and Acoustics* **124**(4), 576–582.
Ormondroyd, J. [1928] "The theory of the dynamic vibration absorber," *Transactions ASME, Applied Mechanics* **50**, 9–22.
Palmeri, A. and Lombardo, M. [2011] "A new modal correction method for linear structures subjected to deterministic and random loadings," *Computers and Structures* **89**(11–12), 844–854.
Petrini, F., Giaralis, A. and Wang, Z. [2020] "Optimal tuned mass-damper-inerter (TMDI) design in wind-excited tall buildings for occupants' comfort serviceability performance and energy harvesting," *Engineering Structures* **204**, 109904.
Pietrosanti, D., De Angelis, M. and Basili, M. [2017] "Optimal design and performance evaluation of systems with tuned mass damper inerter (TMDI)," *Earthquake Engineering and Structural Dynamics* **46**(8), 1367–1388.
Smith, M. C. [2020] "The inerter: A retrospective," *Annual Review of Control, Robotics, and Autonomous Systems* **3**, 361–391.
Sun, H., Zuo, L., Wang, X., Peng, J. and Wang, W. [2019] "Exact h2 optimal solutions to inerter-based isolation systems for building structures," *Structural Control and Health Monitoring* **26**(6), e2357.
Wagg, D. J. [2021] "A review of the mechanical inerter: Historical context, physical realisations and nonlinear applications," *Nonlinear Dynamics* **114**(1), 13–34.
Warburton, G. B. [1982] "Optimum absorber parameters for various combinations of response and excitation parameters," *Earthquake Engineering and Structural Dynamics* **10**(3), 381–401.
Zhang, W. and Li, J. [2001] "Global analysis for a nonlinear vibration absorber with fast and slow modes," *International Journal of Bifurcation and Chaos* **11**(08), 2179–2194.
Zilletti, M., Elliott, S. J. and Rustighi, E. [2012]"Optimisation of dynamic vibration absorbers to minimise kinetic energy and maximise internal power dissipation," *Journal of Sound and Vibration* **331**(18), 4093–4100.